# Polarimetric Analysis of Reverberation Times for 94 GHz Indoor Communication

Brecht Hanssens[1], Maria-Teresa Martínez-Inglés[2], Emmeric Tanghe[1], David Plets[1], José-María Molina-García-Pardo[3], Claude Oestges[4], Luc Martens[1], and Wout Joseph[1]
[1] WAVES, Ghent University, Belgium. e-mail: brecht.hanssens@intec.ugent.be
[2] University Center of Defense, Universidad Politécnica de Cartagena, Spain
[3] SiCoMo, Universidad Politécnica de Cartagena, Spain.
[4] ICTEAM, Université Catholique de Louvain, Belgium.

***Abstract*—This paper presents a measurement-based analysis of both the specular- and dense multipath components (SMC and DMC) at 94 GHz in an indoor environment. A total of 15 positions were measured with a virtual antenna array system, from which we have calculated Power Delay Profiles (PDP). A method was developed that allowed for the full-polarimetric estimation of the specular propagation paths, after which the remainder was regarded as the diffuse spectrum. The behavior of the reverberation time, known from the theory of room electromagnetics, was analyzed based on this diffuse spectrum.**

***Index Terms*–Channel Modeling, Channel Sounding, 94 GHz, mmWave, Polarization, SMC, DMC, Reverberation Time.**

## I. Introduction

Over the recent years, the W-band of the electromagnetic spectrum, ranging from 75 GHz to 110 GHz, has received considerable attention with the continuously-expanding demand for higher data rates. Since the lower frequency bands below 6 GHz are becoming heavily-utilized, new and unused frequency bands are being investigated. The W-band offers a license-free part of the spectrum to overcome these issues, and is primarily used for satellite communications, millimeter-wave radar, and tracking applications for body-centric and short-range distances.

In October 2003, the Federal Communications Commission (FCC) ruled that the frequency spectrum from 92 GHz to 95 GHz was to be made available for high-density fixed wireless services, boosting scientific research around this topic. Presently, only very few studies aim to investigate the indoor propagation characteristics of this frequency band, of which the first narrow- and wideband results can be found in [1] and [2], respectively. In [3], wideband measurement results are presented over the entire W-band, but are limited to a distance of less than 0.5 m. Therefore, this work aims to overcome these gaps in the literature by presenting wideband propagation characteristics of the 94 GHz band in an indoor environment, with distances between transmitter and receiver up to 6 m.

The novelty of this work is that we present a method which is capable of estimating the specular propagation paths from polarimetric radio channel measurement data. We have applied this method for the processing of channel sounding measurement data in the 94 GHz band, leading to the first analysis of reverberation times in this frequency band ever, known from the theory of room electromagnetics [4].

## II. Measurements

### A. Measurement environment

The channel sounding measurements were carried out in a laboratory of the Technical University of Cartagena, Spain. In Figure 1, the measurement scenario is depicted, in which one fixed position acts as the receiver (marked as $ULA_{1..5}$), whilst the transmitter occupies various positions across this room (for a total of 15 uniformly distributed positions, marked 1 to 15).

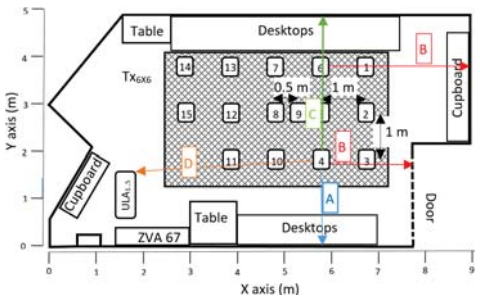


**Figure 1:** Measurement scenario.

The laboratory size is approximately $8\times4.8\times3.5$ meters (see also Figure 1), and it is furnished with several cupboards, chairs, and tables on which numerous computers and electronic devices stand. The walls are typical interior walls, made of plasterboard, whilst the floor and ceiling are made of concrete.

### B. Channel sounding procedure

In order to obtain the channel transfer function, a Vector Network Analyzer (VNA) of type Rohde & Schwarz (R&S) ZVA67 was used to measure the complex radio channel gain (also known as the $S_{21}$–scattering parameter) in the indoor millimeter-wave (mmW) channel ranging from 92.5 GHz up to 95.5 GHz, representing the so called 94 GHz band (or mmW-90 band, part of the W-band). At both ends of the measurement system, a virtual antenna array was created by an automated positioning system on which the antennas were mounted. This virtual Multiple-Input Multiple-Output (MIMO) measurement system consists of a $6 \times 6$ Uniform Rectangular Array (URA) at the transmitter and a 5 element Uniform Linear Array (ULA) at the receiver. Both antennas were polarimetric omni-directional, manufactured by Mi-Wave. At each position in

the laboratory, at least two polarization combination measurements were performed, being either horizontal Tx and horizontal Rx (denoted HH) or vertical Tx and vertical Rx (denoted VV). Some positions also featured the full polarimetric radio channel (HH, HV, VH and VV) between Tx and Rx.

The VNA then measured the complex gain between each combination of transmit- and receive antennas in the virtual array by sampling the 94 GHz band over $M_f = 1024$ uniformly spaced frequency points. Further information about this channel sounding procedure can be found in [5].

## III. Evaluation

### A. Propagation path detection

In order to detect a propagation path, we first calculate the Average Power Delay Profile (APDP) from the measurement data for each possible combination of polarizations $XY$ by performing an inverse discrete Fourier transform (IDFT) on the original signal between each of the $M_T \times M_R = [6 \times 6] \times 5 = 180$ separate Tx- and Rx antennas at a single measurement position. We then average all PDPs to construct an APDP, in order to reduce the influence of the small-scale fading. Since we limit our search for propagation paths to that part of the radio channel which is unaffected by noise, we only analyze the APDP which is significantly above the noise floor. We therefore take the maximum value of the APDP at those time-delays when all multipath components have been significantly attenuated so that only the sum of all noise sources remains, and take an extra margin of 2 dB into account.

Since our measurement data consists of $N_{pol} = 2$ or 4 different polarizations (remember that each measurement position has both HH- and VV-polarizations, whilst some also have HV and VH), we have enhanced the method in [6] in order to take the APDP for each combination of polarizations into account. This results in a joint estimation (w.r.t. polarization) of the propagation paths, ensuring that we extract the same paths over the different polarizations. The search for propagation paths was done by finding the local maxima in the APDP, by comparing the power of the APDP in each delay bin $n$ with a threshold function $T(n)$. This function is basically the local average value of the APDP in a sliding window around each delay bin, and can be mathematically defined as follows:

$$T_{XY}(n) = \frac{\epsilon}{\Delta} \sum_{n-\Delta/2}^{n+\Delta/2} P_{XY}(n), \tag{1}$$

in which $\Delta$ is the length of a sliding window over the time-delay, and $\epsilon$ is an offset of 1 dB in order to overcome detecting power peaks caused by noise or strong diffuse multipath. In our work, we iterate over $\Delta$ values of 3, 7, and 11 delay bins, corresponding with a spatial length of 0.2, 0.6 and 1 m over which the threshold function is calculated, respectively. In this work, we define a specular propagation paths as a distinguishable peak in the APDP, assumed to be originating from a strong path between transmitter and receiver. These paths are located at those time-delays which have a power greater than the threshold value for each polarization combination $XY$. They can thus be defined by a time-delay value and a corresponding power. Because measurements with different polarizations were performed independently, the position of a peak in the APDP could be detected in an adjacent delay bin between e.g., the HH- and VV-data. That is, the polarization of the antennas was changed 90 degrees from horizontal to vertical, or vice versa, between each set of measurements, which could lead to small displacements between the peaks in the APDP of each polarization combination. In order to overcome this issue, we took a margin of one delay bin into account for the detection of a peak in the APDP of all polarizations. More specifically, this means that for each peak in one of $p \in N_{pol}$ different polarizations, we compared the jointly-detected values with the original stored peak values for each polarization.

After the detection of a certain number $L$ of propagation paths in the first iteration over different $\Delta$ values of the sliding window, we reconstruct the PDP $P_{SMC,XY}$ originating from these $L$ paths as performed in [6]. This reconstructed PDP is then subtracted from the measurement data, after which the remainder is again investigated for new paths. This was done in order to possibly detect new paths that were previously obscured by adjacent (stronger) ones. After executing this method until there are no new paths found anymore, and doing so for different $\Delta$ lengths of the sliding window, the remainder of the APDP is regarded as the diffuse spectrum.

### B. Diffuse spectrum modeling

The model for the diffuse spectrum $P_{DMC,XY}(\tau)$ in Eq. (2) is based on the observation that the APDP has a base time-delay $\tau_d$ related to the distance between the transmitter and receiver, together with an exponential decay over time-delay caused by multiple reflections and scattering, corrupted with Gaussian white noise. Note that we compute a separate diffuse spectrum for each of the $p \in N_{pol}$ different polarizations, but have dropped the sub-index $XY$ for visual simplicity.

$$P_{DMC}(\tau) = \begin{cases} \alpha_1 \, e^{\left(-\frac{\tau-\tau_d}{\tau_r}\right)} + \alpha_0, & \text{if } \tau > \tau_d \\ \alpha_0, & \text{otherwise.} \end{cases} \tag{2}$$

The parameters $\alpha_1$, $\tau_d$, $\tau_r$ and $\alpha_0$ were obtained by fitting the above model to the diffuse spectrum, obtained after removal of the estimated propagations paths from our measurement data.

## IV. Results

### A. Power delay profiles

By defining $p_{r,XY}$ as the ratio between the power $P_{XY}$ of the total measured APDP, to the power $P_{SMC,XY}$ attributable to specular paths for each polarization combination $XY$, we can analyze how much power in the channel originates from these specular propagation paths, and how much can be attributed to diffuse powers.

From Figure 2, we can see that the specular co-polar (HH and VV) path powers dominate the diffuse powers for small Tx-Rx distances. This effect becomes slightly less noticeable at larger Tx-Rx distances, where the ratio reduces from 90% to

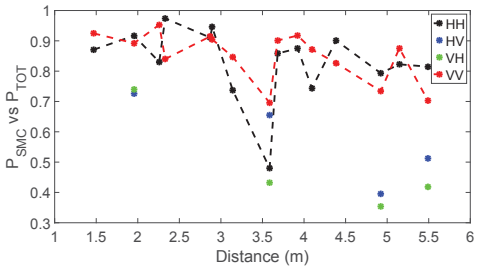


**Figure 2:** Power of propagation paths versus total power.

around 80%, on average. The influence of the specular cross-polar (HV and VH) path powers is lower compared to the diffuse powers, especially at increasing Tx-Rx distances. This is presumably since these cross-polarized channels at large Tx-Rx distance concern more de-polarized components in the channel, and thus more reflected paths, leading to an increased diffuse behavior since their peak values are more difficult to detect. The power of the co-polar specular components thus dominates those of the diffuse components, as they represent up to 80% and more of the total power in the channel.

### *B. Diffuse spectrum*

The reverberation time was estimated from the APDP by performing a regression analysis on the exponential power decay of the diffuse spectrum, which was performed in a dB-scale where this corresponds with a linear power decay. The regression was carried out between the mean power delay bin (the delay bin corresponding with the mean power value), and the noise delay bin [7]. By taking the mean power delay bin, we can reduce the influence of the strong line-of-sight components. These are typically present earlier on in the time-delay domain in the APDP, and might still be noticeable in the part that is regarded as the diffuse spectrum. The reverberation time as a function of distance is shown in Figure 3.

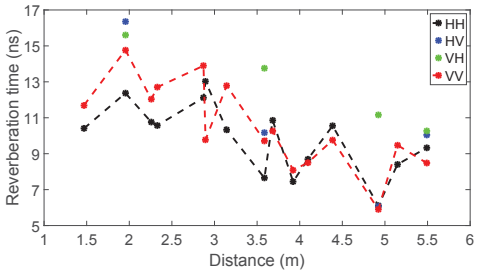


**Figure 3:** Reverberation time.

From Figure 3, we can state that the reverberation time is lower for the co-polarized channels than for the cross-polarized channels, indicating a slower power decay for the diffuse spectrum of the latter. This hints towards more path loss for the cross-polarizations than for the co-polarizations, since the former also include the leakage of polarization due to antenna mismatching and scattering in the environment. The reverberation time for the HH-polarized channel is also noticeably lower than for the VV-polarized channel. This would suggest that more transmitted H-polarized waves penetrate the walls, with less H-polarized reflections back into the room. On the contrary, more transmitted V-polarized waves scatter back into the room with the same polarization. This effect can be identified especially for smaller transmitter-receiver distances.

Our results also show that there is no uniform distribution of power across the room, since the reverberation time depends on the distance between transmitter and receiver. This was validated by calculating the correlation coefficients between the Tx-Rx distances and the corresponding reverberation times, which were -0.57, -0.96, -0.98 and -0.73 for the HH-, HV-, VH-, and VV-polarizations, respectively. The p-values associated with these coefficients were lower than 0.05.

## V. Conclusion

This work presents a method which enables the full-polarimetric estimation of specular propagation paths from Multiple-Input Multiple-Output measurement data. It separates the data into specular- and dense multipath components (SMC and DMC). This method was then applied in an indoor environment at 94 GHz by performing a frequency-domain channel sounding procedure. Our results suggests that the theory of room electromagnetics is not applicable at 94 GHz for this environment, since the contribution of SMC dominates the total power in the channel. Next to that, the reverberation time was found to be heavily dependent on transmitter-receiver distance, indicating that the necessary condition of a rich scattering environment was not met.

## Acknowledgment

Brecht Hanssens is funded by the Agency for Innovation by Science and Technology in Flanders (IWT). Emmeric Tanghe is a Post-Doctoral Fellow of the Research Foundation Flanders (FWO). This research was supported by the FWO project G027714N, IAP BESTCOM and COST CA15104 IRACON.

## References

[1] A. Kajiwara. Indoor Propagation Measurements at 94 GHz. In *IEEE International Symposium on Personal, Indoor and Mobile Radio Communications (PIMRC). Wireless: Merging onto the Information Superhighway*, volume 3, pages 1026–1030, 1995.

[2] J. Helminger, J. Detlefsen, and H. Groll. Propagation Properties of an Indoor-Channel at 94 GHz. In *International Conference on Microwave and Millimeter Wave Technology Proceedings*, pages 9–14, 1998.

[3] R. Piesiewicz, R. Geise, M. Jacob, J. Jemai, and T. Kurner. Indoor Channel Measurements of Point-to-Point Ultra Broadband Short Range Links Between 75 GHz and 110 GHz. In *Antennas and Propagation Society International Symposium (APS)*, pages 1–4, 2008.

[4] J. B. Andersen, J. O. Nielsen, G. F. Pedersen, G. Bauch, and M. Herdin. Room Electromagnetics. *IEEE Antennas and Propagation Magazine (MAP)*, 49(2):27–33, 2007.

[5] M.-T. Martínez-Inglés, D. P. Gaillot, J. Pascual-Garcia, J.-M. Molina-García-Pardo, J.-V. Rodríguez, L. Rubio, and L. Juan-Llácer. Channel Sounding and Indoor Radio Channel Characteristics in the W-band. *EURASIP Journal on Wireless Communications and Networking*, (1):1–8, 2016.

[6] K. Haneda, S. L. H. Nguyen, J. Järveläinen, and J. Putkonen. Estimating the Omni-Directional Pathloss From Directional Channel Sounding. In *10th European Conference on Antennas and Propagation (EuCAP)*, pages 1–5, 2016.

[7] G. Steinböck, T. Pedersen, B. H. Fleury, W Wang, and R Raulefs. Distance Dependent Model for the Delay Power Spectrum of In-room Radio Channels. *IEEE Transactions on Antennas and Propagation (TAP)*, 61(8):4327–4340, 2013.